Study of the X-ray source populations in the galaxy M 83 with *XMM-Newton*

Lorenzo Ducci[1], Manami Sasaki[1],
Frank Haberl[2], Wolfgang Pietsch[2],
Alexandre Kuranov[3], Konstantin Postnov[3]

[1] **Institut für Astronomie & Astrophysik, Tübingen**
[2] **Max-Planck-Institut für extraterrestrische Physik, Garching**
[3] **Sternberg Astronomical Institute, Universitetski, Moscow**

27 June 2011

EBERHARD KARLS UNIVERSITÄT TÜBINGEN

This research is funded by the Deutsche Forschungsgemeinschaft through the Emmy Noether Research Grant SA 2131/1

M 83: general properties

- type: SBc(s) (Sandage & Tammann 1987);
- distance: 4.5 Mpc (Thim et al. 2003);
- apparent dimensions: $12'.9 \times 11'.5$;
- $\sim$face-on ($i \approx 24^\circ$, Talbot et al. 1979).

M83 is experiencing starbust activity:

- star formation induced by the encounter with the dwarf galaxy NGC 5253 (Bohlin et al. 1983)
- present-day star formation rate (SFR): $3 - 4 M_\odot / yr$ (Boissier 2005);

M 83: star formation activity

M83 can be divided in three regions:

Nuclear region ($d_c < 300$ pc):

- SF started ≈ 10-30 Myr ago (Harris et al. 2001).

Optical disk ($d_c \lesssim 7.5$ kpc):

- the star formation activity in the disk has recently dropped;
- SF started ≈ 30 Myr (Jensen et al. 1981).

Outer disk ($7.5 < d_c < 20$ kpc):

- *GALEX* discovered a star forming activity in the outer disk of M 83 (Thilker et al. 2005);
- the star formation in this region has not been an exclusively recent phenomenon: the cluster formation has been ongoing for at least 1 Gyr (Dong et al. 2008).

M 83: star formation activity

M83 can be divided in three regions:

Nuclear region ($d_c < 300$ pc):

- SF started ≈10-30 Myr ago (Harris et al. 2001).

Optical disk ($d_c \lesssim 7.5$ kpc):

- the star formation activity in the disk has recently dropped;
- SF started ≈30 Myr (Jensen et al. 1981).

Outer disk ($7.5 < d_c < 20$ kpc):

- *GALEX* discovered a star forming activity in the outer disk of M 83 (Thilker et al. 2005);
- the star formation in this region has not been an exclusively recent phenomenon: the cluster formation has been ongoing for at least 1 Gyr (Dong et al. 2008).

M 83: star formation activity

M83 can be divided in three regions:

Nuclear region ($d_c < 300$ pc):

- SF started $\approx$ 10-30 Myr ago (Harris et al. 2001).

Optical disk ($d_c \lesssim 7.5$ kpc):

- the star formation activity in the disk has recently dropped;
- SF started ≈ 30 Myr (Jensen et al. 1981).

Outer disk ($7.5 < d_c < 20$ kpc):

- *GALEX* discovered a star forming activity in the outer disk of M 83 (Thilker et al. 2005);
- the star formation in this region has not been an exclusively recent phenomenon: the cluster formation has been ongoing for at least 1 Gyr (Dong et al. 2008).

M 83: star formation activity

M83 can be divided in three regions:

Nuclear region ($d_c < 300$ pc):

- SF started $\approx$10-30 Myr ago (Harris et al. 2001).

Optical disk ($d_c \lesssim 7.5$ kpc):

- the star formation activity in the disk has recently dropped;
- SF started ≈ 30 Myr (Jensen et al. 1981).

Outer disk ($7.5 < d_c < 20$ kpc):

- *GALEX* discovered a star forming activity in the outer disk of M 83 (Thilker et al. 2005);
- the star formation in this region has not been an exclusively recent phenomenon: the cluster formation has been ongoing for at least 1 Gyr (Dong et al. 2008).

XMM-Newton observation of M 83

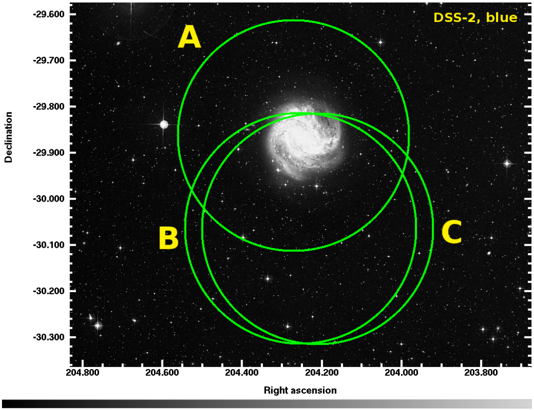

	Obs. ID.	Date	$T_{\rm exp}$ [*ksec*]
A	0110910201	2003-01-27	30.672
B	0503230101	2008-01-16	36.906
C	0552080101	2008-08-16	29.814

X-ray sources in nearby galaxy fields:

- foreground stars;
- background objects (galaxies, galaxy clusters, AGN);

Sources within galaxy:

XRBs:

HMXBs:
- short lifetime $\sim 10^7$ yrs;
- tracer of SF;

LMXBs:
- long lifetime $\gtrsim 10^9$ yrs;
- tracer of mass;

- powerlaw, diskbb;
- $L_\mathrm{x} \approx 10^{35} - 10^{38}\,\mathrm{erg\,s^{-1}}$

SNRs:
- optically-thin thermal plasma at ≈ 0.5 keV;
- $L_\mathrm{x} \lesssim 10^{38}\,\mathrm{erg\,s^{-1}}$

SSSs:
- Nuclear burning WD binaries;
- bbody $kT \approx 15 - 100$ eV
- $L_\mathrm{x} \approx 10^{36} - 10^{38}\,\mathrm{erg\,s^{-1}}$

ULXs:
- accreting intermediate mass BH ($\gtrsim 100\,\mathrm{M}_\odot$);
- found in high SF environments;
- $L_\mathrm{x} > 10^{39}\,\mathrm{erg\,s^{-1}}$

Aims:

1. Study of the X-ray populations in M 83;
2. Calculation of the X-ray Luminosity Function (XLF) of XRBs;
3. Comparison with the XLF of a *simulated binary population* in M 83, using the new-"Scenario Machine";

The "Scenario Machine" is a computer code based on Monte Carlo method for modelling the evolution of binary systems (Lipunov et al. 2009).

The comparison with a synthetic XLF allows to understand the SF history of M 83

Data analysis, source detection

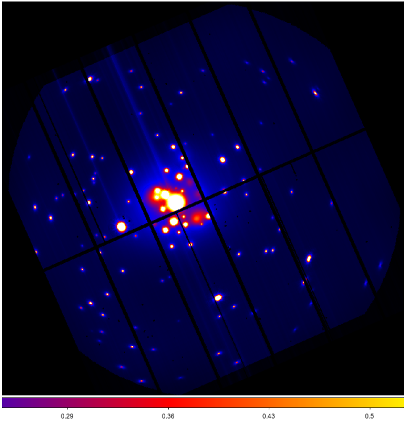

→ event files for PN, MOS1, MOS2;
→ images ∀ instr. in 5 energy bands:

1. 0.2-0.5 keV
2. 0.5-1 keV
3. 1-2 keV
4. 2-4.5 keV
5. 4.5-12 keV

Source detection

- search for significant sources (detection likelihoods $L = \ln p \geq 6$);
- ∀ source, the *source detection* provides several parameters.

Data analysis, source detection

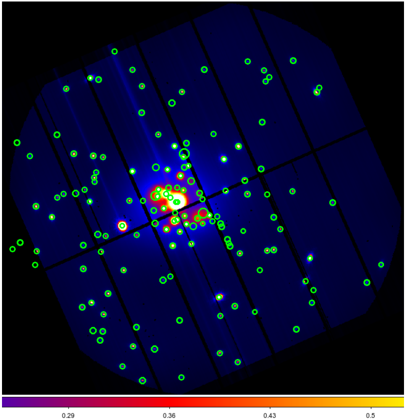

→ event files for PN, MOS1, MOS2;
→ images ∀ instr. in 5 energy bands:

1. 0.2-0.5 keV
2. 0.5-1 keV
3. 1-2 keV
4. 2-4.5 keV
5. 4.5-12 keV

Source detection

- search for significant sources (detection likelihoods $L = \ln p \geq 6$);
- ∀ source, the *source detection* provides several parameters.

source detection applied to 3 observations: ⇒ 218 sources
(fg stars, AGN, bg galaxies, SNRs, XRBs, ULXs, SSSs)

background sources:

- We cross-correlated *XMM-Newton* sources with SIMBAD and NED data base in order to identify bg sources;
- We identified 8 bg galaxies:

Galaxies:			
No.	RA	Dec	Name
6	204.191	-29.987	6dFGS gJ133645.8-295913
39	204.242	-29.851	CXOU J133658.3-295105
72	204.372	-29.841	6dFGS gJ133729.5-295028
73	204.387	-29.850	ESO 444-85
84	204.249	-30.016	BRK2009 7
87	204.365	-30.041	6dFGS gJ133727.5-300228
177	204.064	-29.966	CXO J133615.6-295755
198	204.020	-30.142	QSO B1333-298

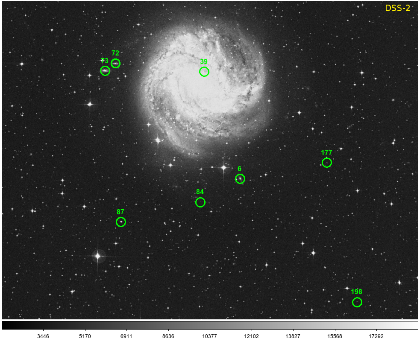

foreground stars

- Cross correlation with optical (USNO-B1, Monet et al. 1998) catalogue;
- The identification with an optical object is confirmed using DSS maps;
- f_x/f_{opt} vs HR diagrams:
  - $\log_{10}(f_x/f_{opt}) = \log_{10}(f_x) + m_B/2.5 + 5.37$ (Maccacaro et al. 1988)
  - Bayesian Estimation of HRs (with BEHR, Park et al. 2006):

  $\longrightarrow$ especially useful in the Poisson regime of low counts;

  $\longrightarrow$ uncertainties well computed even if the source is not detected in both en. bands.

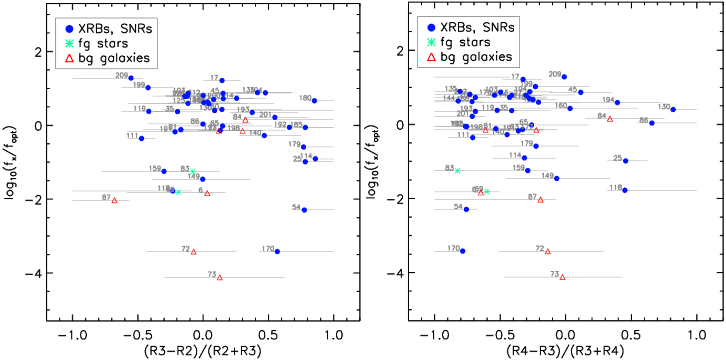

$\Rightarrow$ 4 fg objects identified.

foreground stars

- Cross correlation with optical (USNO-B1, Monet et al. 1998) catalogue;
- The identification with an optical object is confirmed using DSS maps;
- f_x/f_{opt} vs HR diagrams:
  - $\log_{10}(f_x/f_{opt}) = \log_{10}(f_x) + m_B/2.5 + 5.37$ (Maccacaro et al. 1988)
  - Bayesian Estimation of HRs (with BEHR, Park et al. 2006):

  $\rightarrow$ especially useful in the Poisson regime of low counts;

  $\rightarrow$ uncertainties well computed even if the source is not detected in both en. bands.

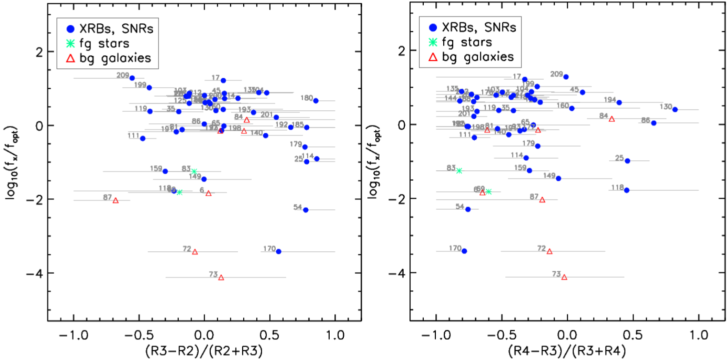

$\Rightarrow$ 4 fg objects identified.

foreground stars

- Cross correlation with optical (USNO-B1, Monet et al. 1998) catalogue;
- The identification with an optical object is confirmed using DSS maps;
- f_x/f_{opt} vs HR diagrams:
  - $\log_{10}(f_x/f_{opt}) = \log_{10}(f_x) + m_B/2.5 + 5.37$ (Maccacaro et al. 1988)
  - Bayesian Estimation of HRs (with BEHR, Park et al. 2006):

  → especially useful in the Poisson regime of low counts;

  → uncertainties well computed even if the source is not detected in both en. bands.

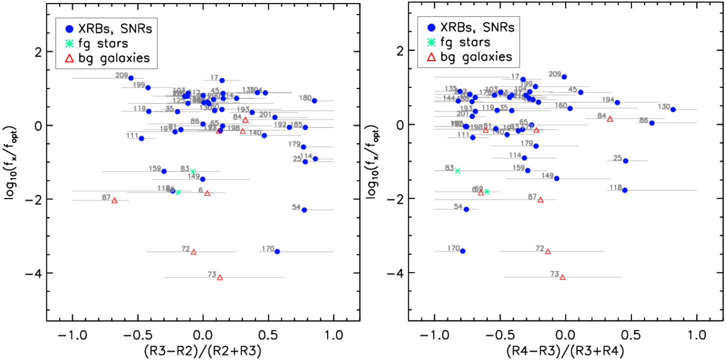

⇒ 4 fg objects identified.

Source classifications

1. Cross-correlation with X-ray catalogues (*Einstein*, *ROSAT*, *Chandra*);
   - $\Rightarrow$ *Einstein*, Trinchieri et al. (1985): 4 sources;
   - $\Rightarrow$ *ROSAT*, Ehle et al. (1998): 29 sources;
   - $\Rightarrow$ *ROSAT*, Immler et al. (1999): 27 sources;
   - $\Rightarrow$ *Chandra*, Soria & Wu (2002-2003): 37 sources;
   - $\Rightarrow$ total: 64 sources;
2. New classifications:
   - cross-correlation with optical and radio source catalogues;
     - $\Rightarrow$ optical, Blair & Long (2004): $\sim$ 3 SNRs;
     - $\Rightarrow$ radio, Maddox et al. (2006), NVSS: 5 sources;
   - X-rays properties:
     - hardness ratios $\longrightarrow$ color-color diagrams;
     - X-ray variability;
     - spectral analysis (only bright sources);

Source classifications

1. Cross-correlation with X-ray catalogues (*Einstein*, *ROSAT*, *Chandra*);
   - ⇒ *Einstein*, Trinchieri et al. (1985): 4 sources;
   - ⇒ *ROSAT*, Ehle et al. (1998): 29 sources;
   - ⇒ *ROSAT*, Immler et al. (1999): 27 sources;
   - ⇒ *Chandra*, Soria & Wu (2002-2003): 37 sources;
   - ⇒ total: 64 sources;
2. New classifications:
   - cross-correlation with optical and radio source catalogues;
     - ⇒ optical, Blair & Long (2004): ~ 3 SNRs;
     - ⇒ radio, Maddox et al. (2006), NVSS: 5 sources;
   - X-rays properties:
     - hardness ratios → color-color diagrams;
     - X-ray variability;
     - spectral analysis (only bright sources);

Source classifications

1. Cross-correlation with X-ray catalogues (*Einstein*, *ROSAT*, *Chandra*);
   - ⇒ *Einstein*, Trinchieri et al. (1985): 4 sources;
   - ⇒ *ROSAT*, Ehle et al. (1998): 29 sources;
   - ⇒ *ROSAT*, Immler et al. (1999): 27 sources;
   - ⇒ *Chandra*, Soria & Wu (2002-2003): 37 sources;
   - ⇒ total: 64 sources;
2. New classifications:
   - cross-correlation with optical and radio source catalogues;
     - ⇒ optical, Blair & Long (2004): ~ 3 SNRs;
     - ⇒ radio, Maddox et al. (2006), NVSS: 5 sources;
   - X-rays properties:
     - hardness ratios → color-color diagrams;
     - X-ray variability;
     - spectral analysis (only bright sources);

Color-color diagrams

Useful tool to study spectral properties of faint sources
and separate sources into groups dominated by one or 2 source types.

We calculated:

1. grid of spectral models:
   - XRBs: powerlaw or DISKBB;
   - SNRs: thermal plasma model (NEI);
   - SSSs: blackbody;
   - $10^{20} \leq N_{\mathrm{H}} \leq 2 \times 10^{22}\,\mathrm{cm}^{-2}$
2. bayesian HRs ∀ source:

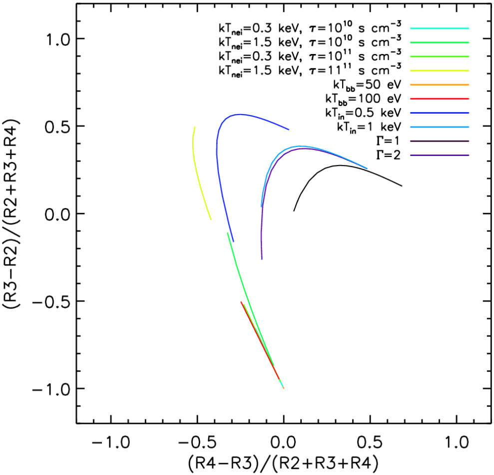

Color-color diagrams

Useful tool to study spectral properties of faint sources
and separate sources into groups dominated by one or 2 source types.

We calculated:

1. grid of spectral models:
   - XRBs: powerlaw or DISKBB;
   - SNRs: thermal plasma model (NEI);
   - SSSs: blackbody;
   - $10^{20} \leq N_{\mathrm{H}} \leq 2 \times 10^{22}$ cm^{-2}
2. bayesian HRs $\forall$ source

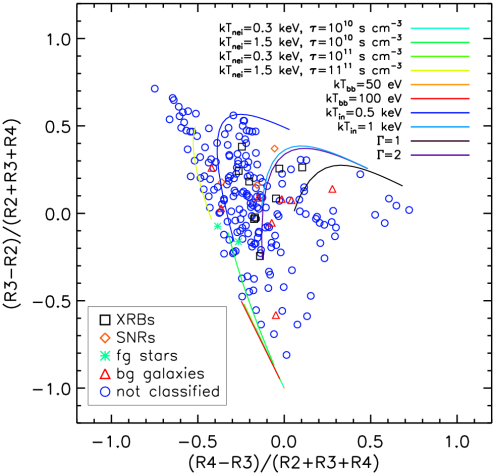

Color-color diagrams

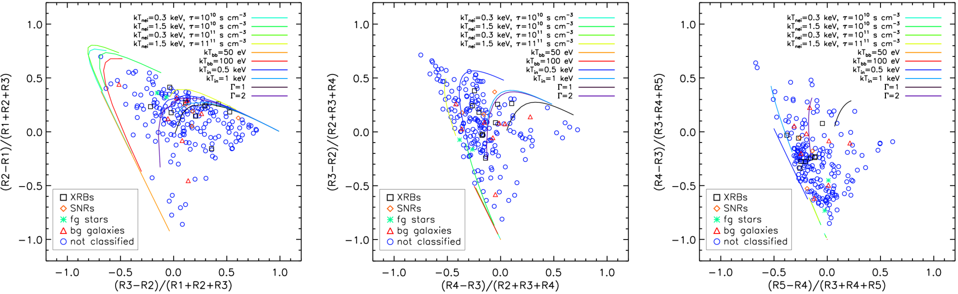

Color-color diagrams

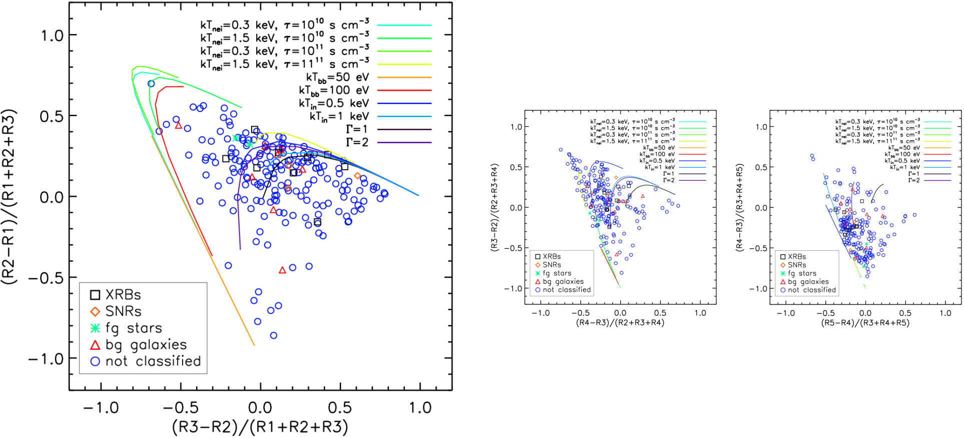

→ SSSs and ∼SNRs

R1: 0.2 – 0.5 keV R2: 0.5 – 1 keV R3: 1 – 2 keV

Color-color diagrams

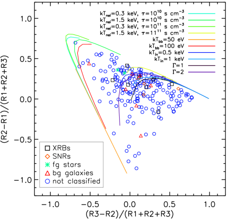

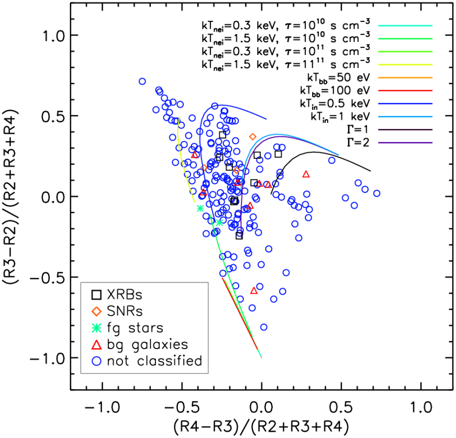

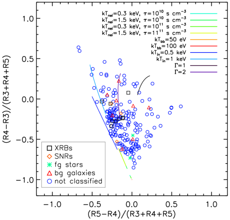

→ XRBs and ∼ SNRs

R2: 0.5 – 1 keV R3: 1 – 2 keV R4: 2 – 4.5 keV

Color-color diagrams

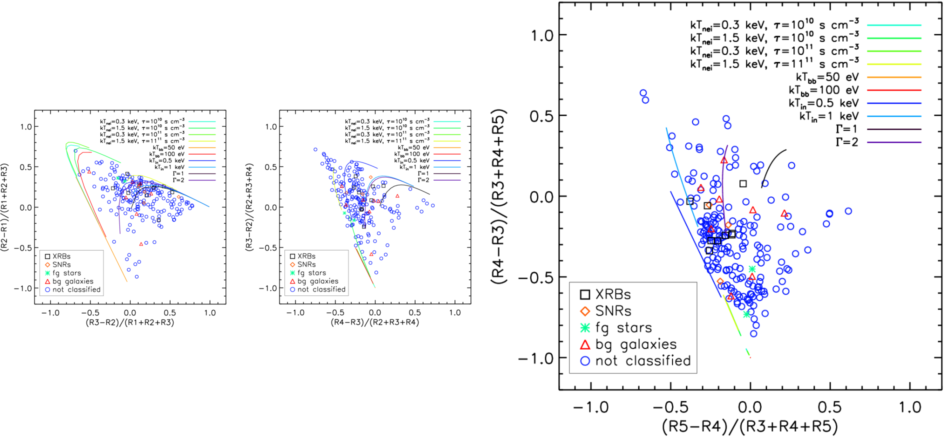

$\sim$ hard XRBs

R3: 1 – 2 keV R4: 2 – 4.5 keV R5: 4.5 – 12 keV

X-ray variability

Long-term flux variability:
- used to further constrain the nature of X-ray sources;
- ∀ obs. and source, we calculated the average flux or upper-limit (0.2-4.5 keV);
- Variability factor: $V_{\rm f} = F_{\rm max}/F_{\rm min}$.

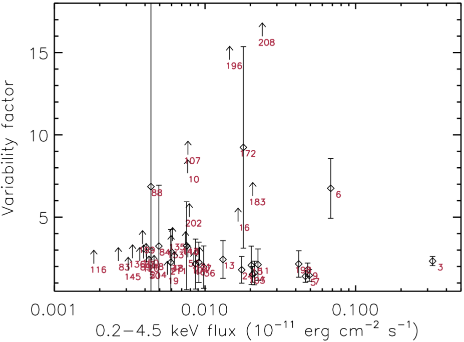

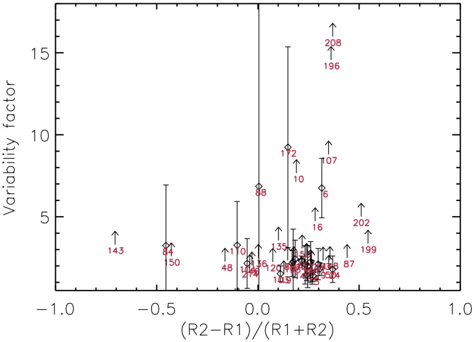

The XLF of M 83

We considered two new energy bands:

- $0.3 - 2\,\mathrm{keV}$;
- $2 - 10\,\mathrm{keV}$.

We calculated the XLFs for two regions of M 83:

- "inner disk" ($< D25$ ellipse);
- "outer disk" ($> D25$ ellipse);
- total XLF:
  (inner + outer disk).

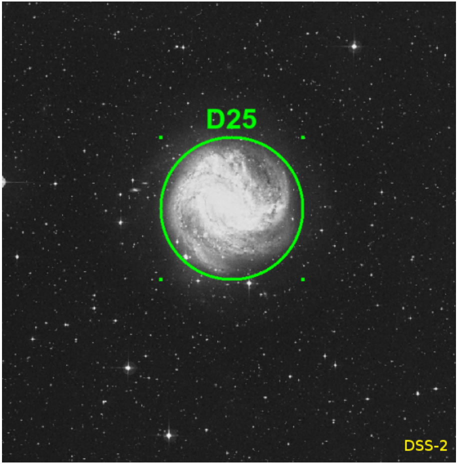

OBS.A (M 83 in the center of the *XMM-Newton* FOV):

1. XLF obtained subtracting SNRs, SSSs, fg stars, bg objects;

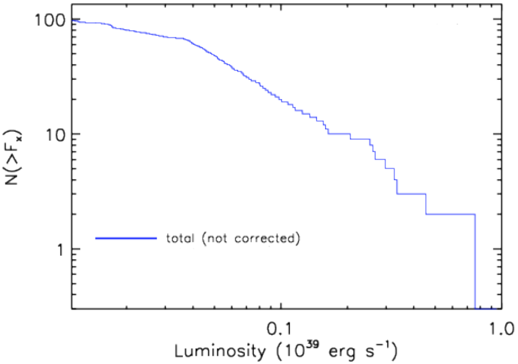

OBS.A (M 83 in the center of the *XMM-Newton* FOV):

1. XLF obtained subtracting SNRs, SSSs, fg stars, bg objects;
2. correction for incompleteness

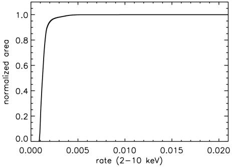

$$N(>S) = \sum_{i=1}^{N_s} \frac{1}{\Omega_i} \, \mathrm{deg}^{-2}$$

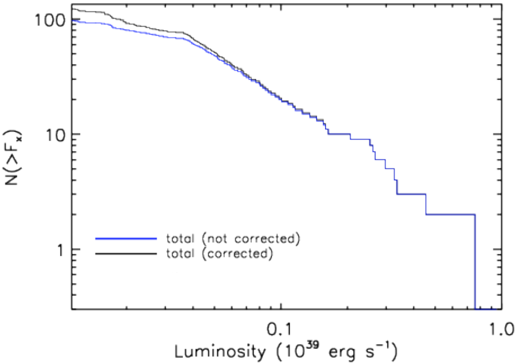

OBS.A (M 83 in the center of the *XMM-Newton* FOV):

1. XLF obtained subtracting SNRs, SSSs, fg stars, bg objects;
2. correction for incompleteness

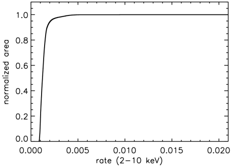

$$N(>S) = \sum_{i=1}^{N_s} \frac{1}{\Omega_i} \,\mathrm{deg}^{-2}$$

3. bg-corrected XLF; we subtracted the AGN distribution of Cappelluti et al. (2009)

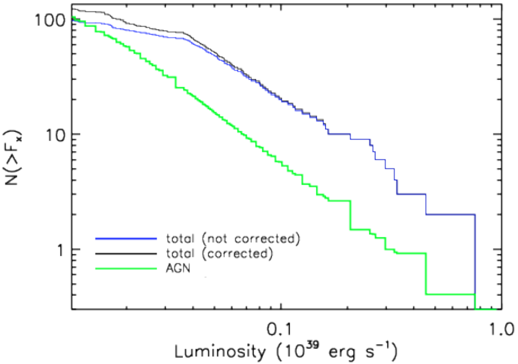

OBS.A (M 83 in the center of the *XMM-Newton* FOV):

1. XLF obtained subtracting SNRs, SSSs, fg stars, bg objects;
2. correction for incompleteness

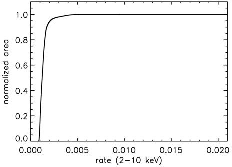

$$N(>S) = \sum_{i=1}^{N_s} \frac{1}{\Omega_i} \deg^{-2}$$

3. bg-corrected XLF; we subtracted the AGN distribution of Cappelluti et al. (2009)

Jump to skycov slide

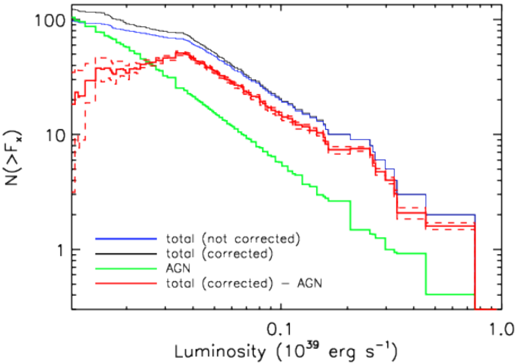

XLFs: observation A

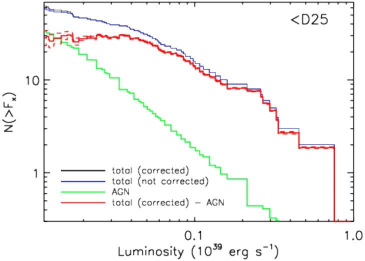

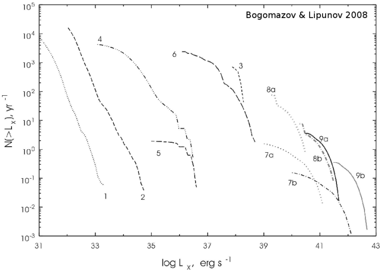

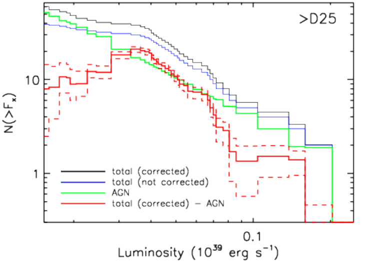

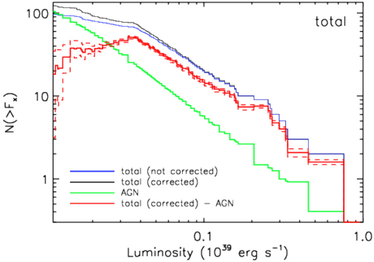

XLFs: observation B

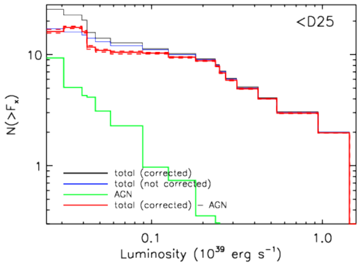

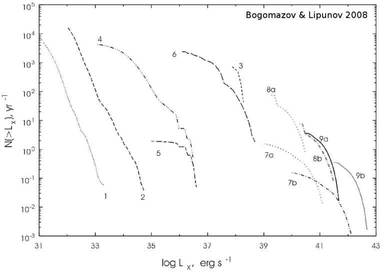

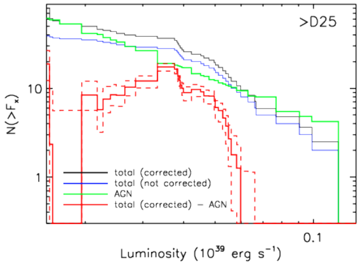

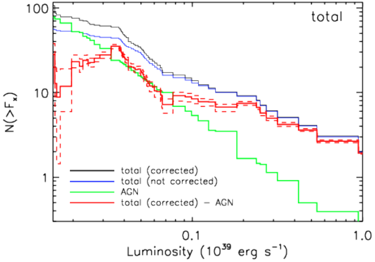

XLFs: observation C

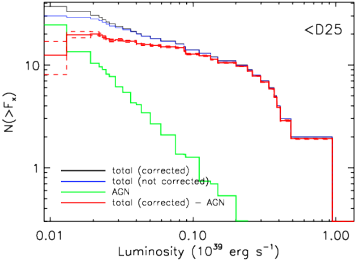

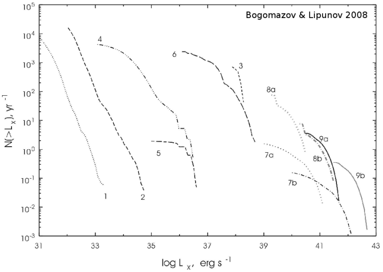

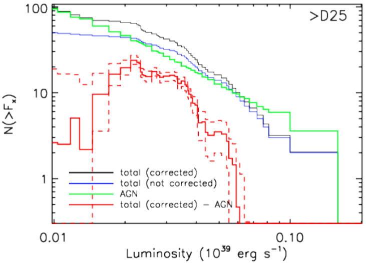

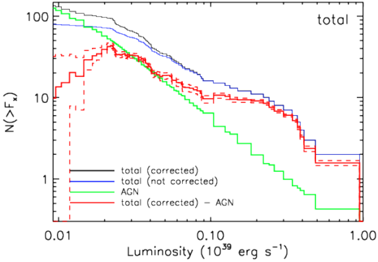

Summary

Results:

- We detected 218 sources in 3 *XMM-Newton* observations of the starburst galaxy M 83;
- We identified the population of XRBs by means of:
  - color-color diagrams;
  - X-ray variability;
  - spectral variability (only for a few sources);
  - association with optical/radio counterparts;
- XLFs ($2 - 10$ keV) show the presence of X-ray objects belonging to M 83, in the outer disk (in agreement with the discovery of Bigiel et al. 2010 from *GALEX* observations);

Future work:

- Calculate the XLF in the energy range $0.3 - 2$ keV;
- Comparison with the theoretical XLF obtained with the new-"Scenario Machine";
- Study of the diffuse emission in M 83.

thanks!

Bayesian hardness ratios

- Bayesian method does not allow for a simple analytic solution similar to the standard error propagation in the Gaussian case.
- Park et al. (2006) implemented:
    1. Monte-Carlo integration method *(Gibbs sampler)*:
       $\longrightarrow$ the estimates have simulation errors in addition to the true variability $\longrightarrow$ to reduce the errors: many iterations;
    2. analytic method, based on numerical integration *(quadrature)*:
       $\longrightarrow$ if the number of counts is large, the computation becomes expensive.

Gibbs method is faster, but it needs a sufficient number of iterations (we used 100000);
$\Rightarrow$ *Gibbs* for high counts;
$\Rightarrow$ *Quadrature* for low counts.

Sky coverage function

- Exposure time, background and PSF are not uniform across the FOV of *XMM-Newton*

⇒ The sensitivity to source detection varies significantly across the FOV: only bright sources can be detected over the entire area, whereas at faint fluxes the effective area decreases.

- We calculated the Sky coverage function, i.e. the effective area as a function of flux:

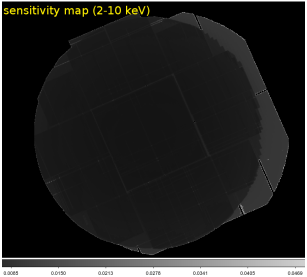

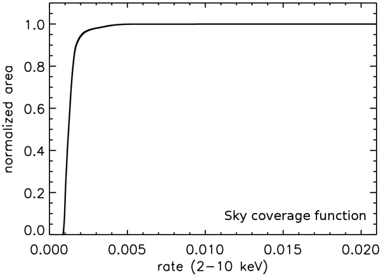

$$N(>S) = \sum_{i=1}^{N_s} \frac{1}{\Omega_i} \deg^{-2}$$

- N_s: number of sources with flux $> S$;
- Ω_i: sky coverage associated with the flux of the ith source.